Chapter 3

A Highly Stable and Efficient Quasi-Solid-State Dye Sensitized Solar Cell Based on Poly(methyl methacrylate)/Carbon Black Polymer Gel Electrolyte with Improved Open-Circuit Voltage

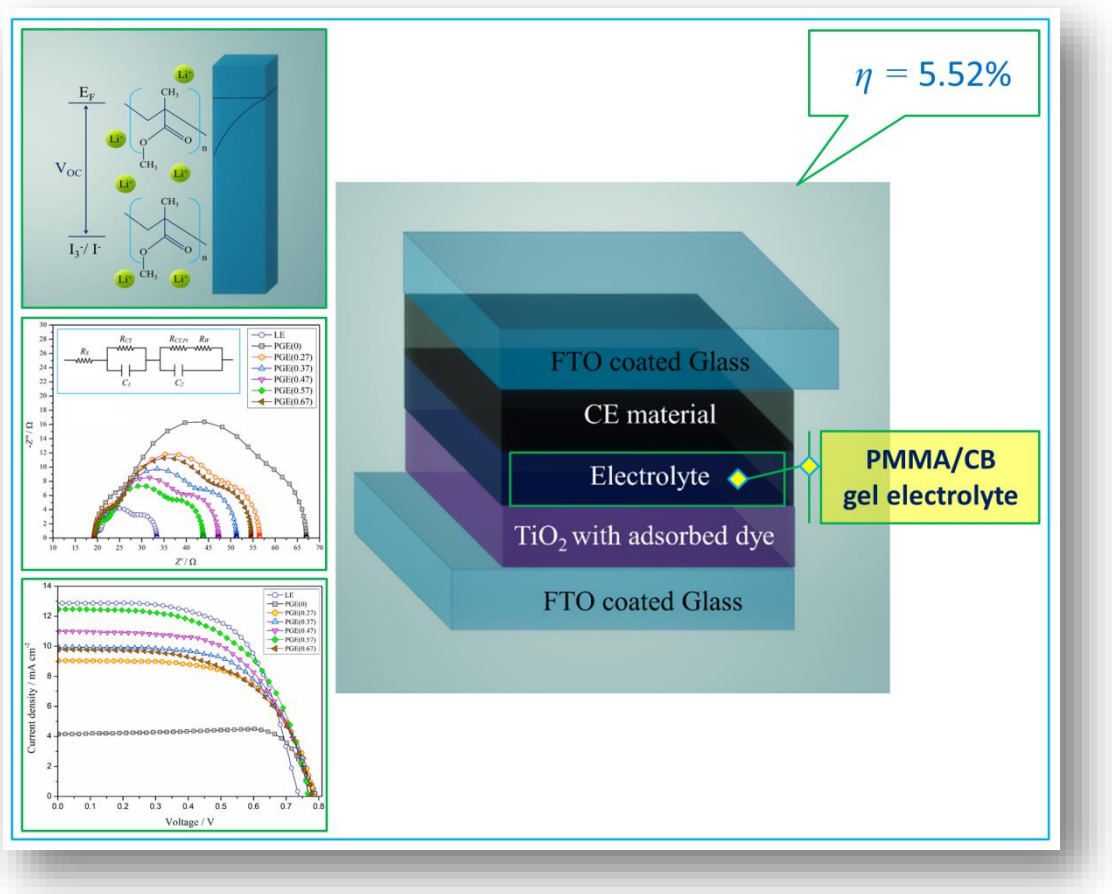

DSSC based on PMMA/CB blend PGE gives an efficiency of 5.52%, wherein CB helps in improving the ionic conductivity of the gel electrolyte to increase the magnitude of J_{SC} and PMMA enhances the V_{OC} value by restricting the movement of Li^+ ions in the polymer matrix.

3.1 Introduction

In the present study, poly(methyl methacrylate) (PMMA) based polymer gel electrolyte (PGE) is used for fabrication of durable dye sensitized solar cell (DSSC). The ionic conductivity of the PGE is optimized using different weight percentages (wt%) of a conductive material, nano-sized mesoporous carbon black (CB) (<500 nm particle size), and their effect on the efficiency enhancement of the fabricated DSSCs is studied. The charge transfer kinetics at the TiO_2/electrolyte interface is studied to analyze the open-circuit voltage (V_{OC}) values, while the charge transfer at the platinum counter electrode is studied using incident photon-to-current efficiency (IPCE) spectra. In addition, the durability of the fabricated DSSCs are also tested and analyzed.

Many successful DSSCs have been developed using PGEs exhibiting long-term stability with significant photoconversion efficiency [1–14]. In 1995, Cao et al. reported the first DSSC fabricated with thermoplastic PGE exhibiting an overall conversion efficiency of 4.4% [13]. This quasi-solid-state cell exhibited transient behavior similar to that of DSSC fabricated with liquid electrolyte. Marchezi et al. reported a poly(ethylene oxide) (PEO) based gel electrolyte with reduced graphene oxide as additive which exhibited photoconversion efficiency of 5.07% [15].

Usually in case of PGE, ionic mobility of ions and charge transfer kinetics between the gel electrolyte and the electrodes are lower in comparison to the liquid electrolyte at room temperature. By introducing a small amount of conducting nanomaterials as additives the charge transfer kinetics can be enhanced. Carbon based materials like graphite powder, graphene nano-sheet and reduced graphene oxide have been already reported as additives in the polymer matrix to improve the photoconversion efficiency [15–17].

This part of the thesis is published in:

Mohan, K., Dolui, S., Nath, B. C., Bora, A., Sharma, S., and Dolui, S. K. A highly stable and efficient quasi solid state dye sensitized solar cell based on Polymethyl methacrylate (PMMA)/Carbon black (CB) polymer gel electrolyte with improved open circuit voltage. *Electrochimica Acta*, 247:216-228, 2017.

3.2 Experimental section

3.2.1 Materials

Carbon black (CB) was purchased from Aldrich. All the other materials used for the experiments were same as mentioned in Section 2.2.1 of Chapter 2.

3.2.2 Preparation of PMMA/CB based polymer gel electrolytes

PMMA was prepared by free radical polymerization of methyl methacrylate described in Section 2.2.2 of Chapter 2. The liquid electrolyte was first prepared by adding 0.5 M lithium iodide, 0.05 M iodine, 0.5 M t-butyl pyridine and 0.6 M 1-methyl 3-propylimidazolium iodide in a solvent mixture of acetonitrile and N-methyl 2-pyrrolidone (NMP) (volume ratio 8:2), followed by stirring this mixture until no solid was observed. The PGEs were prepared by dispersing different wt% of CB and PMMA into the liquid electrolyte. PGEs based on PMMA with wt% 0, 0.27, 0.37, 0.47 and 0.57 CB were designated as PGE(0), PGE(0.27), PGE(0.37), PGE(0.47) and PGE(0.57), respectively. These prepared PGEs were subsequently used to fabricate the DSSCs.

3.2.3 DSSC fabrication

A clean fluorine doped tin oxide (FTO) coated glass sheet was treated with titanium tetrachloride ($TiCl_4$) solution. Then a paste of titanium dioxide (TiO_2) was deposited on the pre-treated FTO glass *via* doctoral blade method. Subsequently, the glass sheet was dipped in N719 dye solution to obtain the dye adsorbed TiO_2 photoanode. Chloroplatinic acid (H_2PtCl_6) was spin coated onto a clean FTO glass and reduced with sodium borohydride ($NaBH_4$) to fabricate the platinum (Pt) counter electrode. The detailed electrode preparation techniques are given in Section 2.2.5 of Chapter 2.

Finally, the DSSCs with different PGEs were fabricated by placing the PGEs in between the TiO_2 photoanode and the Pt counter electrode using 25 µm thick Solaronix thermal polymer spacers. The internal spacer gap between the two electrodes was completely filled by the gel electrolyte. To improve the interfacial contact between the gel electrolyte and the electrodes, the fabricated prototype devices were kept at 60°C for 5 min [18–20].

3.2.4 Characterization

ZEISS field emission scanning electron microscope (FE-SEM) was used to study the surface morphologies of different PGEs. A Shimadzu 2450 UV–visible spectrophotometer was used to study the absorption patterns of different gel electrolytes. A solar simulator with xenon arc lamp (AM 1.5, 100 mW cm^{-2}) was used to provide 1 sun illumination. The photocurrent density-

voltage (*J-V*) characteristics under illumination were record to evaluate the photovoltaic performance of the DSSCs. The electrochemical impedance spectroscopy (EIS) data was recorded at 0.75 V bias potential by sandwiching the gel electrolyte between two stainless steel electrodes with a space gap (25 µm) from 25°C to 60°C to investigate the temperature dependence of the ionic conductivities of the PGEs. The ionic conductivity was calculated by using **Eq. (2.1)** given in Chapter 2. EIS data was also recorded under illumination and fitted with an equivalent circuit to investigate the various charge transfer resistances of the gel electrolytes with frequency range from 1 MHz to 0.1 Hz at amplitude of 10 mV. The obtained spectra were fitted and analyzed by using Z-view software. The electron diffusion coefficients of the electrolytes were also calculated by fitting the EIS data with the equivalent circuit.

3.3 Results and discussion

3.3.1 FE-SEM analysis

The surface morphology of the different PGEs was studied by using FE-SEM. A wavy surface is observed in the PMMA polymer without liquid electrolyte (**Figure 3.1(a)**). In the **Figure 3.1(b)**, PGE without CB exhibits a rough surface. The surfaces of these PGEs gradually become porous with the incorporation of CB (**Figure 3.1(c)-(g)**). However, agglomeration of CB in the PMMA matrix is observed in the sample containing 0.67 wt% CB resulting in a less porous morphology.

3.3.2 Photovoltaic performance

The *J-V* characteristics of the DSSCs employing liquid electrolyte and PGEs under irradiation of 100 mW cm^{-2} light are shown in **Figure 3.2**. The DSSC employing liquid electrolyte exhibits a V_{OC} value of 0.734 V, a short-circuit current density (J_{SC}) value of 12.87 mA cm^{-2} and *FF* value of 0.63, corresponding to a power conversion efficiency (PCE) of 5.96%. The details of the photovoltaic parameter are listed In **Table 3.1**. A noticeable enhancement in V_{OC} is observed for PGEs when compared to the liquid electrolyte. PMMA based PGE without CB (i.e., PGE(0)) shows a V_{OC} value of 0.794 V. The same device shows J_{SC} value of only 4.15 mA cm^{-2} with a PCE of 2.77%. Adding a small amount of CB can improve these values significantly. The optimized DSSC fabricated with PGE(0.57) exhibits the highest PCE of 5.52% with the magnitudes of V_{OC}, J_{SC} and *FF* as 0.766 V, 12.43 mA cm^{-2} and 0.58 respectively. The increase in the J_{SC} value is due to the enhancement of ionic conductivity with the addition of CB (from 0.27 to 0.57 wt%) in PMMA. However, further addition (>0.57 wt %) of CB results in agglomeration and damages the cell performance. PGE(0.67) exhibits smaller current density in

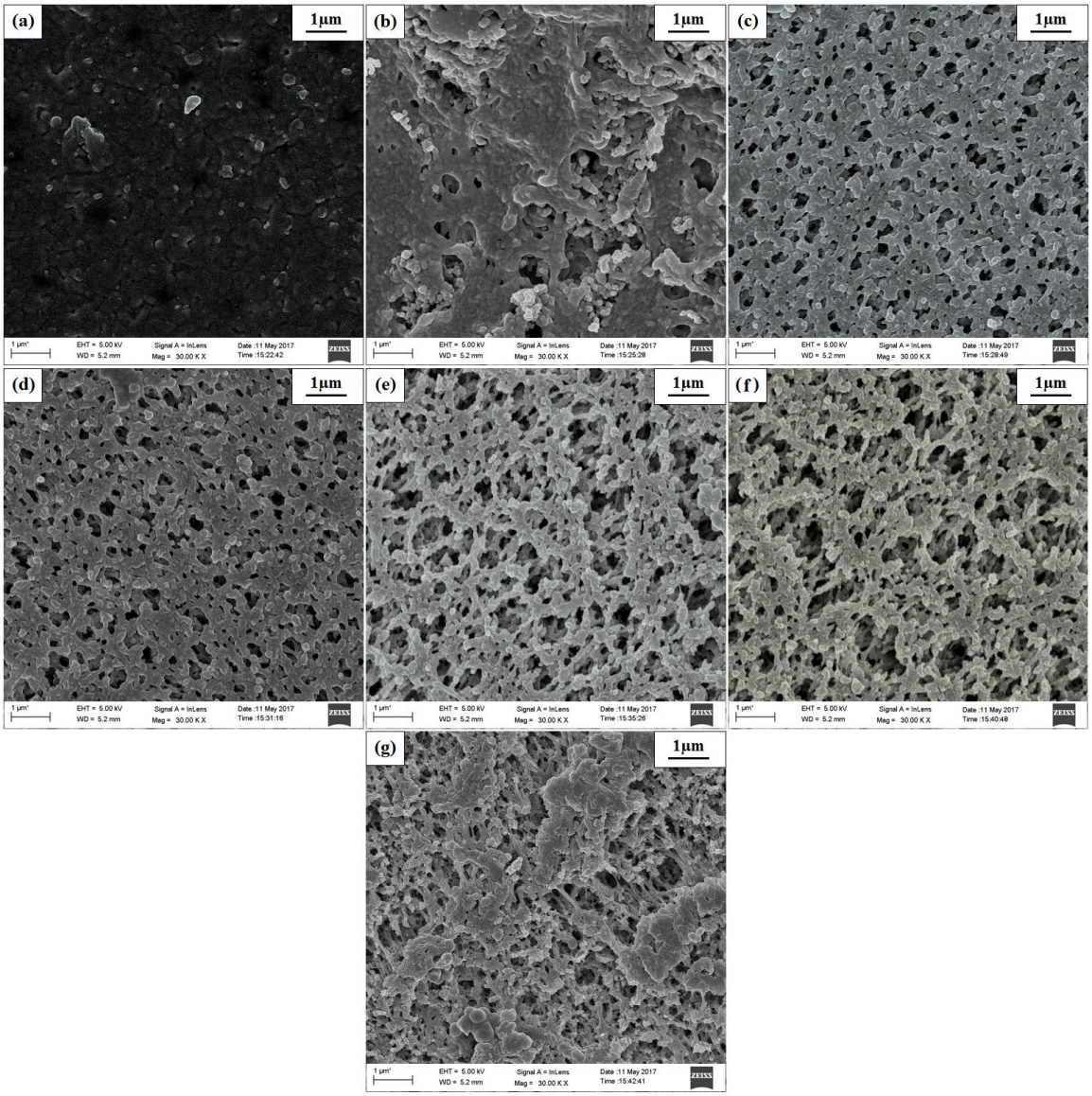

Figure 3.1. FE-SEM images of **(a)** PMMA/CB polymer blend with 0.57 wt% of CB without electrolyte, and PMMA/CB based PGE with **(b)** 0 wt%, **(c)** 0.27 wt%, **(d)** 0.37 wt%, **(e)** 0.47 wt%, **(f)** 0.57 wt% and **(g)** 0.67 wt% of CB.

contrast to the PGE(0.57). This is due to the adsorption of agglomerated CB on the active surface of the Pt counter electrode and the photoanode, resulting in inhibition of the electron transfer kinetics at both the electrode/electrolyte interfaces. Thus the current of PGE(0.67) decreases dramatically because of the hindrance of the electron transfer processes at the interface.

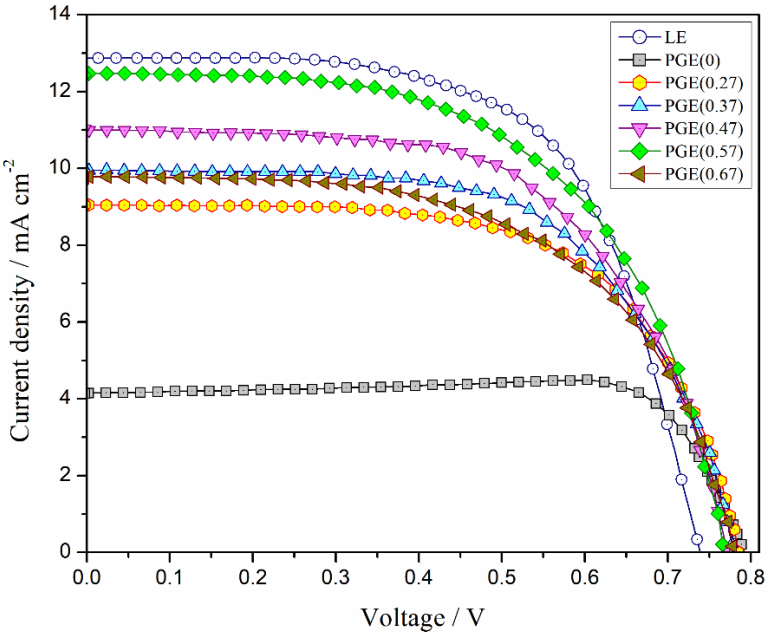

Figure 3.2. *J-V* characteristics of various DSSCs employing liquid electrolyte and PGEs with different wt% of CB in PMMA matrix.

Table 3.1. Photovoltaic parameters of the DSSCs employing liquid electrolyte and different PGEs.

	LE**	**Polymer gel electrolyte**					
		PGE(0)*	PGE(0.27)*	PGE(0.37)*	PGE(0.47)*	PGE(0.57)*	PGE(0.67)*
V_{OC} / V	0.734	0.794	0.785	0.777	0.771	0.766	0.778
J_{SC} / mA cm^{-2}	12.87	4.15	9.05	9.98	11.03	12.43	9.79
FF	0.63	0.84	0.63	0.62	0.60	0.58	0.57
η / %	5.96	2.77	4.49	4.81	5.10	5.52	4.34

** LE stands for liquid electrolyte.

* PGE stands for polymer gel electrolyte and the number within bracket represents the wt% of added CB in the gel electrolyte.

3.3.3 Ionic transport behavior in PGE

The ionic conductivities of the PGEs were measured to investigate the ionic transport behavior. The EIS data were recorded at 25°C, 30°C, 35°C, 40°C, 45°C, 50°C, 55°C and 60°C by applying 0.75 V bias potential to the gel electrolytes sandwiched between two stainless steel electrodes with space gap (25 µm). As the V_{OC} of the fabricated DSSCs were found near 0.75V, the bias potential was set at 0.75 V to record the EIS data. An Arrhenius behavior is observed from the **Figure 3.3**, which can be fitted and analyzed with the **Eq. (2.2)** described in Chapter 2. It is clearly observed that the ionic conductivities increase with the addition of CB. At 298.5 K, the PGE without CB shows conductivity of 9.87×10^{-4} S cm^{-1}, which is increased to 3.32×10^{-3} S cm^{-1} with the addition of 0.57 wt% of CB under same experimental conditions. But PGE(0.67) exhibits significantly lower value of conductivity of 2.59×10^{-3} S cm^{-1}. The activation energies of PGE(0), PGE(0.27), PGE(0.37), PGE(0.47), PGE(0.57) and PGE(0.67) are 25.35, 13.98, 11.46, 10.14, 8.95 and 13.07 kJ mol^{-1} respectively. The results indicate that the charge transport behavior is increased by the addition of CB up to 0.57 wt%. Thus, the PGE behaves like a good ionic transport medium facilitating physical diffusion of ions. Higher ionic conductivity and lower activation energy are helpful in increasing the magnitude of J_{SC} of the fabricated DSSCs [21].

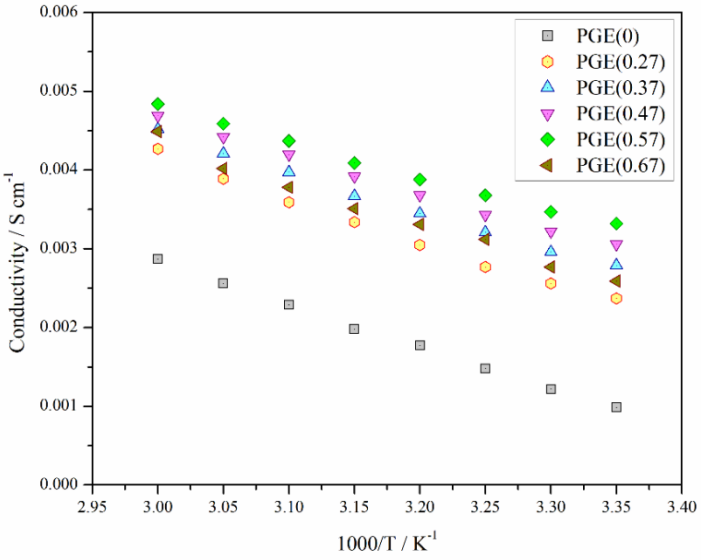

Figure 3.3. Temperature dependence of ionic conductivity of the PGEs with different wt% of CB in PMMA matrix applying bias potential.

3.3.4 Voltage enhancement of the PGEs

J-V characteristics of the DSSCs employing PGEs display a significant enhancement of V_{OC}. The difference between the potential of the quasi Fermi level of TiO_2 (E_F) and the redox potential (E_{redox}) of the triiodide/iodide redox couple under irradiation of light determines the magnitude of the recorded V_{OC}, which can be mathematically expressed as

$$V_{oc} = \frac{kT}{q}\left(\frac{E_c - E_{redox}}{kT} + \ln\frac{n_c}{N_c}\right) \quad \textbf{(3.1)}$$

where q, E_C, k, T, n_c and N_C are the charge, conduction band edge of TiO_2, Boltzmann constant, temperature, free electron density at conduction band of TiO_2 and density of accessible state in the conduction band of TiO_2. E_{redox} is fixed for a particular redox couple, so from the relation (3.1), it can be inferred that the enhancement of V_{OC} is because of either higher E_C or higher n_c values of TiO_2 or both. The magnitude of the n_c is inversely proportional to the recombination kinetics at the photoanode under a given irradiation wavelength. Thus, the value of E_C and the recombination kinetics at the photoanode/electrolyte interface determines the enhancement of the V_{OC} of DSSC fabricated with PGEs [22].

To clarify the influence of PGE on E_C of TiO_2, the chemical capacitances ($C\mu$) of the PGEs were measured using EIS under dark conditions at different applied bias. **Figure 3.4** shows the effect of the applied bias on $C\mu$ of the PGEs. The applied bias acts as the V_{OC} of that DSSC.

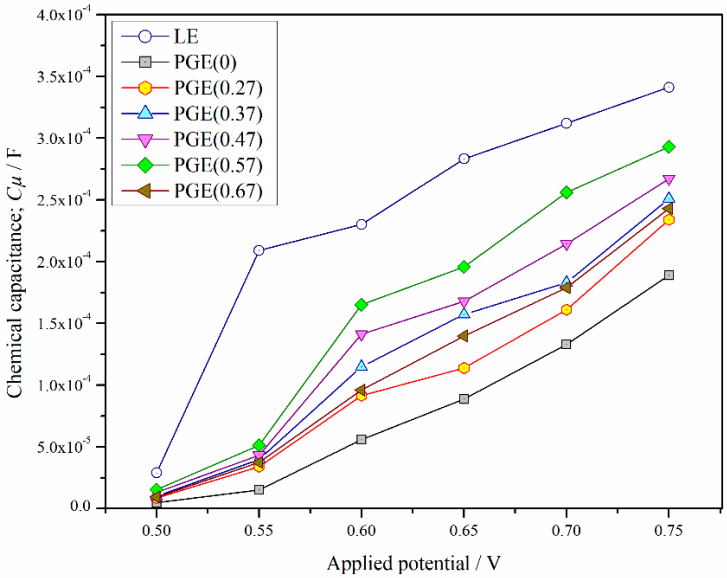

Figure 3.4. Chemical capacitance of liquid electrolyte and different PGEs with various applied potentials.

The electron density generated at the photoanode due to the non-faradic process under the applied potential (bias) determines the value of $C\mu$ which is reflected in the magnitude of E_C of TiO_2. The change in the value of $C\mu$ is equal to the shift of the E_C band for identical geometrical dimensions of the photoanode [22–24]. From the **Figure 3.4**, it is observed that the bias potentials of the PGEs are greater in magnitude in contrast to the liquid electrolyte at a particular capacitance value. It signifies a negative shift of the E_C value for the PGE resulting in improvement of the V_{OC} value. To determine the interfacial charge transfer processes at the TiO_2/electrolyte interface, the dark current characteristics of DSSCs with different electrolytes were recorded under dark conditions. A forward bias is applied, in which electrons are injected into the E_C band of the semiconductor (TiO_2). The injected electrons then reduce the I_3^- ions in the electrolyte by travelling through the mesoporous TiO_2 film. The kinetics of the reduction of the I_3^- ions or the interfacial charge transfer process at photoanode determines the magnitude of the dark current. In **Figure 3.5,** it is seen that the dark current of the liquid electrolyte is higher in contrast to those of the PGEs at a fixed applied potential. This implies that the recombination process in faster for liquid electrolyte than the PGEs. Among all the PGEs, PGE(0) shows the highest dark current and PGE(0.57) exhibits the lowest dark current. But the dark current again increases with further incorporation of CB (0.67 wt%) in the PGE. Hence, the addition of 0.57 wt% CB in the PMMA matrix can optimally suppress the recombination kinetics at the photoanode/electrolyte interface.

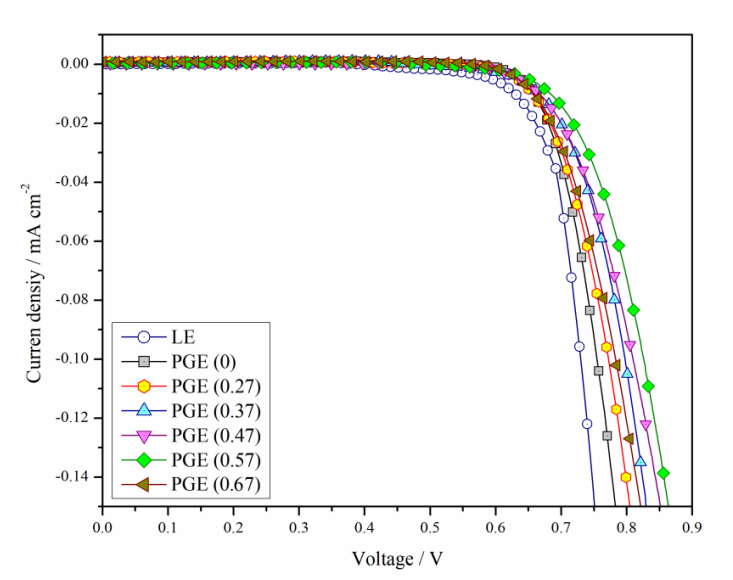

Figure 3.5. *J-V* characteristics of the DSSCs employing liquid electrolyte and PGEs under dark condition.

The effect of the PGE on the interfacial charge transfer processes was further investigated using EIS data under illumination. **Figure 3.6** shows the Nyquist plots (Z' vs $-Z''$) of the recorded

EIS for fabricated DSSCs. Three semicircles can be seen in the Nyquist plos. The semicircle in the high frequency region represents the charge transfer at the Pt counter electrode/electrolyte ($R_{CT,Pt}$) interface, the middle range is assigned to the charge transfer at the TiO_2/electrolyte interface (R_{CT}) and the low frequency region is related to the ionic diffusion in the electrolyte. On the basis of the transmission line model, the EIS data can be fitted with an equivalent circuit to analyze the data as shown in the inset of **Figure 3.6** [25,26].

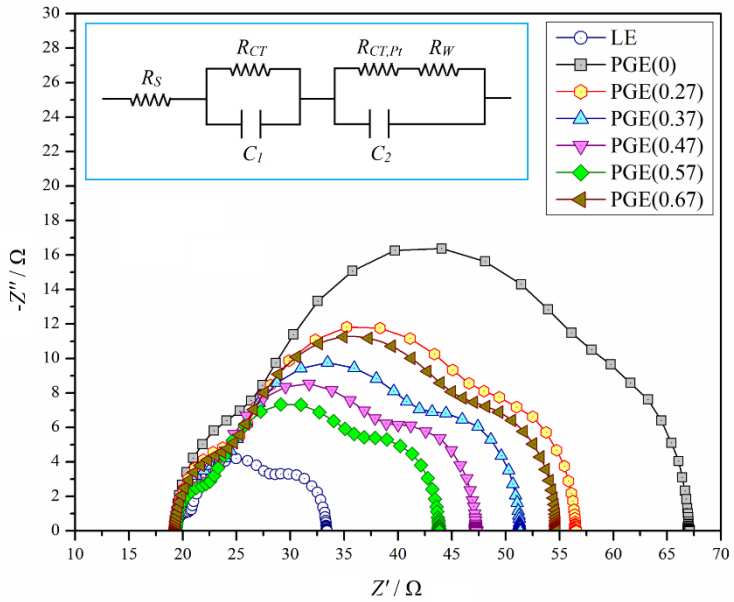

Figure 3.6. EIS plots of the DSSCs employing liquid electrolyte and PGEs with different CB content obtained under irradiation. The inset shows the corresponding equivalent circuit model.

Table 3.2. EIS parameters of the DSSCs employing liquid electrolyte and different PGEs.

	LE**	**Polymer gel electrolyte**					
		PGE(0)*	PGE(0.27)*	PGE(0.37)*	PGE(0.47)*	PGE(0.57)*	PGE(0.67)*
$R_{CT,Pt}$ / Ω	1.47	7.73	6.14	4.91	3.69	3.48	5.65
R_{CT} / Ω	7.35	29.34	21.01	17.18	15.13	12.99	19.98

** LE stands for liquid electrolyte.

* PGE stands for polymer gel electrolyte and the number within bracket represents the wt% of added CB in the gel electrolyte.

To clarify the interfacial charge transfer process, the semicircle in the middle range is considered. The R_{CT} value of the PGEs are higher than that of the liquid electrolyte, indicating

the suppression of recombination kinetics at the photoanode for the DSSC fabricated with PGEs. Moreover, with the increment of CB in the PGEs upto 0.57 wt%, the R_{CT} value decreases as shown in **Table 3.2**. This value increases with further addition of CB (0.67 wt%) in the PGE.

Figure 3.7 exhibits the electron lifetime (τ_{eff}) of the interfacial charge-transfer process involving PGEs. τ_{eff} is measured from the EIS data under illumination by using the **Eq. (3.2)** [27].

$$\tau_{eff} = \frac{1}{k_{eff}} \quad \text{..... (3.2)}$$

where k_{eff} is the rate constant of the interfacial charge transfer process involved at the TiO_2/electrolyte interface. The interfacial charge transfer process is considered as pseudo first-order recombination process, so the rate constant is equal to the frequency corresponding to the peak of the middle semicircle. By substituting the value of the rate constant in **Eq. (3.2)**, the value of τ_{eff} can be easily calculated. From the EIS data and using **Eq. (3.2),** the τ_{eff} values for PGE(0), PGE(0.27), PGE(0.37), PGE(0.47), PGE(0.57) and PGE(0.67) are found as 0.042, 0.036, 0.032, 0.030, 0.027 and 0.035 s respectively. It is observed that τ_{eff} decreases from PGE(0) to PGE(0.57), resulting in fast interfacial charge transfer process. But PGE(0.67) exhibits higher τ_{eff}. This analysis also supports the dark-current characteristics.

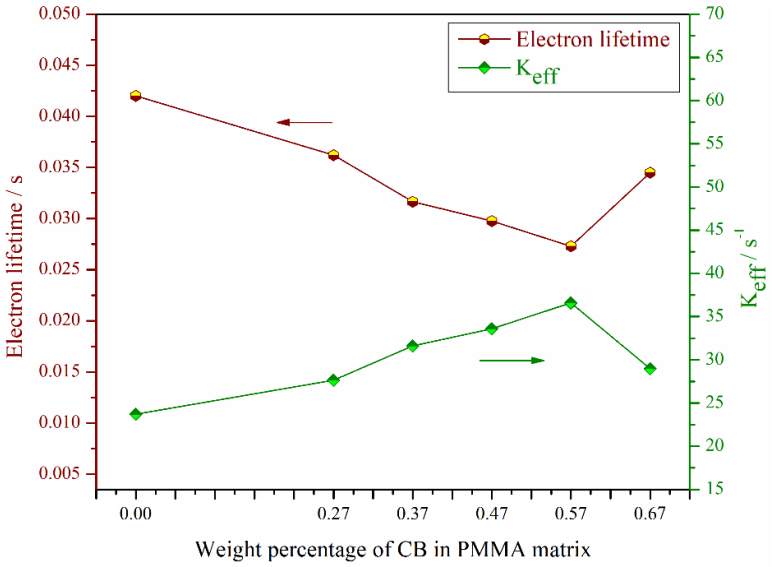

Figure 3.7. Electron lifetime and rate constant for the charge recombination at the photoanode with different wt% of CB in PMMA matrix.

To obtain further insight into the photo-electrochemical properties of the PGEs, their IPCE spectra were studied (**Figure 3.8)** [28]. It is observed that the number of collected electrons increases with the increment of CB (IPCE onset from 45% to 55%) in the PGEs resulting in enhancement of J_{SC}. This result supports the *J-V* characteristics of the DSSCs. **Figure 3.8** also

signifies that a broad wavelength range can also contribute to the improvement of the J_{SC} value for the series of PGEs (0.37-0.57%). The IPCE onset is the ratio of the number of electrons extracted from the device per incident number of photons. There are two factors which determine the IPCE onset: one is the number of extracted electrons and the other is the number of absorbed photons. The number of extracted electrons can be indirectly obtained from the τ_{eff} data at the photoanode/electrolyte interface. The PGE without CB (i.e., PGE(0)) exhibits the highest τ_{eff} value (0.042 s) than the PGEs with different wt% of CB, as shown in **Figure 3.8**. The higher τ_{eff} value increases the charge recombination kinetics at the photoanode, thereby reducing the number of photoexcited electrons. The number of extracted electrons is nothing but the number of photoexcited electrons which can be collected or contribute to the J_{SC} value. Thus, IPCE onset for PGE(0) is the lowest in comparison to the PGEs. PGE(0.57) exhibits the highest IPCE onset because of its lowest τ_{eff} value (0.0273 s).

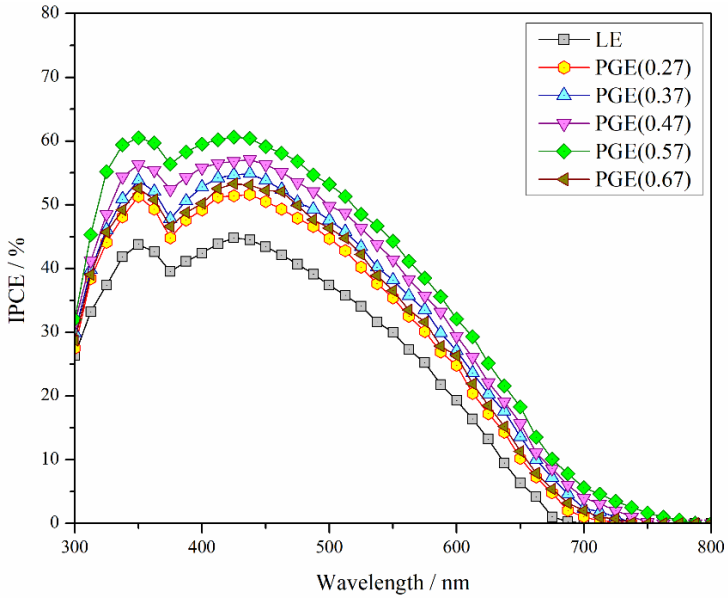

Figure 3.8. IPCE spectra of the PGEs with different wt% of CB.

To study the absorption of the different PGEs, the UV-vis spectra of the prepared PGEs without and with CB were collected (**Figure 3.9**). In this study, an increase in the absorption with the increment of CB in the PGE matrix is seen. This might hinder the absorption of light by the dye molecules. But an improvement of IPCE onset with the addition of CB upto 0.57wt% was obtained in the previous section. This improvement of IPCE onset is due to the suppression of recombination kinetics of the excited electrons of dye molecules resulting in higher number of extracted electrons at the photoanode.

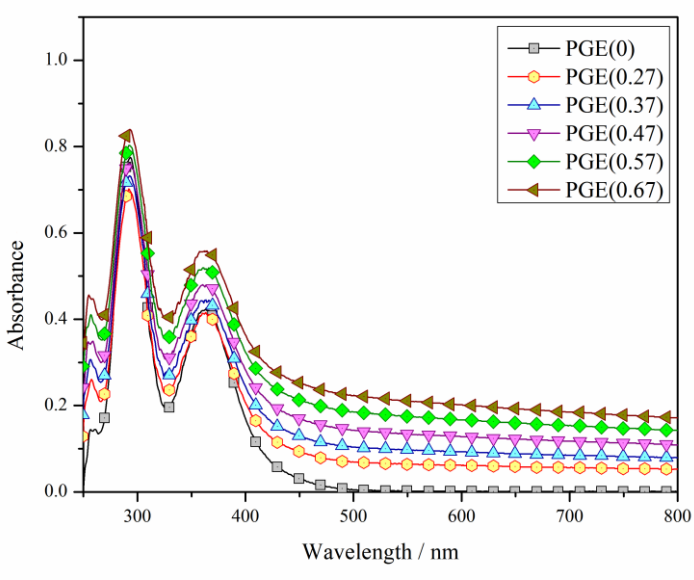

Figure 3.9. UV-vis spectra of PGEs with different wt% of CB.

In conclusion, it is confirmed that the negative shift of the E_C band by PGEs and decrease in the recombination process enhances the V_{OC} of the DSSC fabricated with PGEs. **Scheme 3.1** is used to explain this phenomenon, which is elucidated as follows.

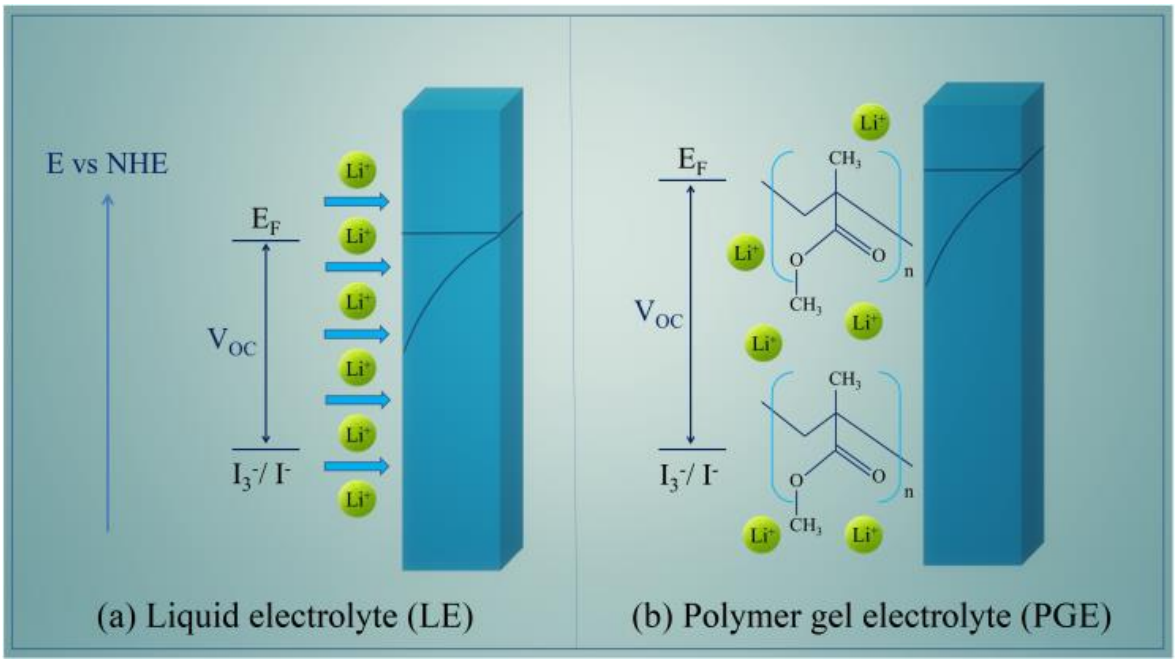

Scheme 3.1. Energy bands and surface states of DSSCs employing **(a)** liquid electrolyte and **(b)** PGE.

Under irradiation of light, the TiO_2 photoanode becomes negatively charged due to injection of electrons from the dye molecules. Consequently, the positively charged Li^+ ions

present in the electrolyte form an electrical double layer at the photoanode surface as a result of the non-faradic process [29–31]. A potential drop is observed because of this, which lower the magnitude of V_{OC} of DSSC fabricated with liquid electrolyte (**Scheme 3.1(a)**). Contrariwise, in case of PGEs, the Li^+ ions might get attracted by the electronically rich oxygen of the ester groups of PMMA. Thus, the non-faradic process of adsorption of Li^+ ions on the photoanode gets suppressed for the PGE due to inhibition of the movement of Li^+ ions in PGE as shown in **Scheme 3.1(b)**. Therefore in case of PGEs, the E_C band edge shifts to a negative position resulting in enhancement of V_{OC}.

3.3.5 Charge transfer process at the Pt counter electrode

The charge transfer process at the Pt counter electrode was studied from the data calculated from the EIS measurements under illumination from the **Figure 3.6**. At the Pt counter electrode, I_3^- ions are reduced by the electrons from the external circuit. The charge transfer kinetics of reduction of I_3^- ions at the Pt surface determines the values of charge transfer resistance ($R_{CT,Pt}$). Hence, the increase in the availability of I_3^- ions at the Pt counter electrode enhances the charge transfer process resulting in lowering of $R_{CT,Pt}$. It is observed from **Table 3.2** that there is a significant difference in $R_{CT,Pt}$ at the interfaces of the Pt counter electrode and the different electrolytes. From the data, it is confirmed that $R_{CT,Pt}$ decreases form PGE(0) to PGE(0.57). It again increases with further addition of CB (0.67 wt%) in the PGE. This is due to the adsorption of agglomerated CB on the active sites of the Pt counter electrode. In case of liquid electrolyte, the magnitude of $R_{CT,Pt}$ is the lowest in contrast to all the PGEs.

The improvement of charge transfer process with the addition of CB in the PMMA matrix is due to the enhancement of diffusion coefficient of the I_3^- ions in the PGEs with the increment of CB content. **Figure 3.10** shows the diffusion coefficient of I_3^- ions calculated from the data obtained from the EIS measurement under illumination. The diffusion coefficients data of I_3^- ions in liquid electrolyte at 25˚C is the highest, having a value of 1.87×10^{-5} cm^{-1} s^{-1}. PGE(0.57), PGE(0.47), PGE(0.37), PGE(0.27) and PGE(0) exhibit diffusion coefficients of 1.64×10^{-5}, 1.41×10^{-5}, 1.06×10^{-5}, 0.92×10^{-5} and 0.79×10^{-5} cm^{-1} s^{-1} respectively. PGE(0.67) has the value of 1.05×10^{-5} cm^{-1} s^{-1}, which is even lower compared to the diffusion coefficient of PGE(0.37). Diffusion coefficient (D) is calculated using the **Eq. (3.3)** [30].

$$D = (1/2.5) l^2 w_{\max} \quad \text{..... (3.3)}$$

where l represents the distance between two electrodes and w_{max} represents the corresponding peak frequency of the semicircle in the lower frequency regions of the Nyquist plot (**Figure 3.6**).

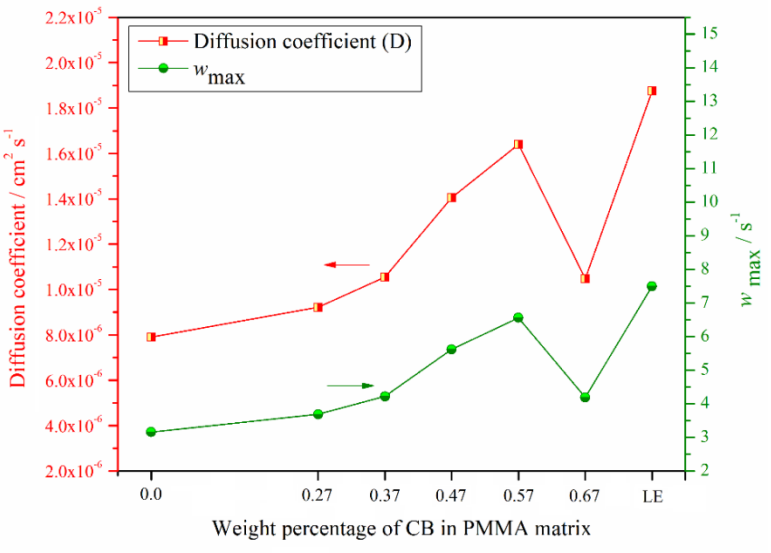

Figure 3.10. Diffusion coefficient of the I_3^- ions and w_{max} values of the liquid electrolyte and the PGEs with different wt% of CB.

3.3.6 Long-term stability of the fabricated DSSCs

Durability of the DSSCs with liquid electrolyte and the gel electrolytes are investigated for duration of 1000 h in air at room temperature. The results are shown in **Figure 3.11**.

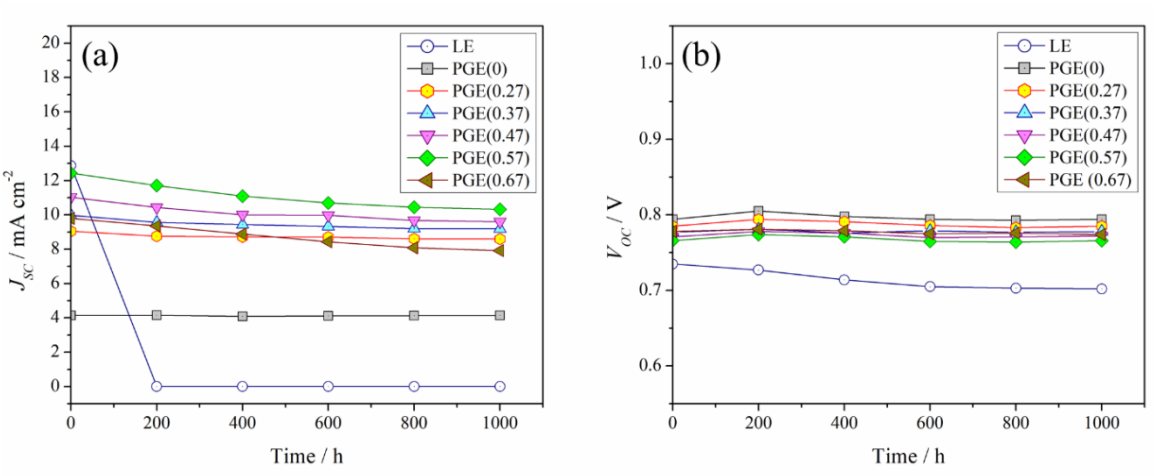

Figure 3.11. (a) J_{SC} and **(b)** V_{OC} values of the DSSCs fabricated with liquid electrolyte and PGEs with different wt% of CB during 1000 h of testing.

The J_{SC} values of the DSSC fabricated with liquid electrolyte decays sharply after 200 h of testing. This is due to the leakage and volatilization of the solvent used in the preparation of the liquid electrolyte. However, the DSSCs fabricated with the PGEs exhibit significant long-term stability as the solvent molecules are trapped in the polymer matrix. After 200h of testing, the J_{SC} values remain almost constant for all the DSSCs. After 1000 h of testing, PGE(0) exhibits similar

J_{SC} value (4.14 mA cm^{-2}). The J_{SC} values for DSSCs with PGE(0.67), PGE(0.57), PGE(0.47), PGE(0.37) and PGE(0.27) are retained at 81, 83, 87, 92 and 95% of their initial performances. Hence, the DSSCs fabricated with PGEs exhibit very good long-term stability in contrast to the DSSC fabricated with liquid electrolyte. It is also observed that the V_{OC} values of the DSSCs devised with both the liquid electrolyte and the PGEs are almost similar. Thus, PMMA/CB based PGEs encumber the leakage and volatilization of solvents from the fabricated DSSCs resulting in a durable cell.

3.4 Conclusion

- A series of PGEs based on PMMA polymer matrix with different wt% of CB were fabricated. The morphological images of the prepared PGEs displayed their porous structures.
- An optimized DSSC fabricated with the PMMA based gel electrolyte with 0.57 wt% CB exhibited the highest efficiency of 5.52 % under irradiation of 100 mW cm^{-2} (AM 1.5) light. V_{OC} value of 0.766 V, J_{SC} value of 12.43 mA cm^{-2} and *FF* value of 0.58 were obtained.
- The J_{SC} values increased with the increment of CB in the PGE. This increase was caused by an enhancement of ionic conductivities and a decrease in the charge transfer resistances at the two electrode/electrolyte interfaces.
- The DSSC fabricated with PGE showed a significant enhancement in V_{OC} (0.766 V) in contrast to the DSSC with liquid electrolyte (0.734 V). The chemical capacitance at the photoanode/PGE interface was lowered by the restricted movement of lithium ions due to the electron rich groups present in the polymer matrix, and this subsequently enhanced the V_{OC} values.
- An improvement of the charge transfer kinetics at the counter electrode/PGE interface was seen with the addition of CB. This was justified by the raise in magnitude of the diffusion coefficient of triiodide ions (*D*) computed form the EIS data.
- The optimized DSSC fabricated with the PGE with 0.57 wt% CB showed a significant long-term stability by retaining 83% of the initial J_{SC} value after 1000 h of testing.

3.5 References

[1] Bach, U., Lupo, D., Comte, P., Moser, J. E., Weissörtel, F., Salbeck, J., Spreitzer, H., and Grätzel, M. Solid-state dye-sensitized mesoporous TiO_2 solar cells with high photon-to-electron conversion efficiencies. *Nature*, 395(6702):583-585, 1998.

[2] Snaith, H. J., and Schmidt-Mende, L. Advances in liquid-electrolyte and solid-state dye-sensitized solar cells. *Advanced Materials*, 19(20):3187-3200, 2007.

[3] Wang, G., Zhou, X., Li, M., Zhang, J., Kang, J., Lin, Y., Fang, S., and Xiao, X. Gel polymer electrolytes based on polyacrylonitrile and a novel quaternary ammonium salt for dye-sensitized solar cells. *Materials Research Bulletin*, 39(13):2113-2118, 2004.

[4] Tu, C. W., Liu, K. Y., Chien, A. T., Lee, C. H., Ho, K. C., and Lin, K. F. Performance of gelled-type dye-sensitized solar cells associated with glass transition temperature of the gelatinizing polymers. *European Polymer Journal*, 44(3):608-614, 2008.

[5] Wang, P., Zakeeruddin, S. M., Moser, J. E., Nazeeruddin, M. K., Sekiguchi, T., and Grätzel, M. A stable quasi-solid-state dye-sensitized solar cell with an amphiphilic ruthenium sensitizer and polymer gel electrolyte. *Nature Materials*, 2(6):402-407, 2003.

[6] Wang, P., Zakeeruddin, S. M., Exnar, I., and Grätzel, M. High efficiency dye-sensitized nanocrystalline solar cells based on ionic liquid polymer gel electrolyte. *Chemical Communications*, 8(24):2972-2973, 2002.

[7] Fabregat-Santiago, F., Bisquert, J., Cevey, L., Chen, P., Wang, M., Zakeeruddin, S. M., and Grätzel, M. Electron transport and recombination in solid-state dye solar cell with spiro-OMeTAD as hole conductor. *Journal of the American Chemical Society*, 131(2):558-562, 2009.

[8] Zakeeruddin, S. M. and Grätzel, M. Solvent-free ionic liquid electrolytes for mesoscopic dye-sensitized solar cells. *Advanced Functional Materials*, 19(14):2187-2202, 2009.

[9] de Freitas, J. N., Nogueira, A. F., and De Paoli, M. A. New insights into dye-sensitized solar cells with polymer electrolytes. *Journal of Materials Chemistry*, 19(30):5279, 2009.

[10] Wang, Y. Recent research progress on polymer electrolytes for dye-sensitized solar cells. *Solar Energy Materials and Solar Cells*, 93(8):1167-1175, 2009.

[11] Wu, J. H., Lan, Z., Lin, J. M., Huang, M. L., Hao, S. C., Sato, T., and Yin, S. A novel thermosetting gel electrolyte for stable quasi-solid-state dye-sensitized solar cells. *Advanced Materials*, 19(22):4006-4011, 2007.

[12] Chen, C. L., Teng, H., and Lee, Y. L. In situ gelation of electrolytes for highly efficient gel-state dye-sensitized solar cells. *Advanced Materials*, 23(36):4199-4204, 2011.

[13] Cao, F., Oskam, G., and Searson, P. C. A solid state, dye sensitized photoelectrochemical

cell. *The Journal of Physical Chemistry*, 99(47):17071-17073, 1995.

[14] Yang, Y., Zhou, C. H., Xu, S., Hu, H., Chen, B. L., Zhang, J., Wu, S. J., Liu, W., and Zhao, X. Z. Improved stability of quasi-solid-state dye-sensitized solar cell based on poly (ethylene oxide)–poly (vinylidene fluoride) polymer-blend electrolytes. *Journal of Power Sources*, 185(2):1492-1498, 2008.

[15] Marchezi, P. E., Sonai, G. G., Hirata, M. K., Schiavon, M. A., and Nogueira, A. F. Understanding the role of reduced graphene oxide in the electrolyte of dye-sensitized solar cells. *Journal of Physical Chemistry C*, 120(41):23368-23376, 2016.

[16] Li, Q., Wu, J., Tang, Q., Lan, Z., Li, P., and Zhang, T. Application of polymer gel electrolyte with graphite powder in quasi-solid-state dye-sensitized solar cells. *Polymer Composites*, 30(11):1687-1692, 2009.

[17] Nath, B. C., Das, D., Kamrupi, I. R., Mohan, K. J., Ahmed, G. A., and Dolui, S. K. An efficient quasi solid state dye sensitized solar cell based on polyethylene glycol/graphene nanosheet gel electrolytes. *RSC Advances*, 5(115):95385-95393, 2015.

[18] Miyamoto, T. and Shibayama, K. Free-volume model for ionic conductivity in polymers. *Journal of Applied Physics*, 44(12):5372-5376, 1973.

[19] Li, Q., Wu, J., Tang, Z., Xiao, Y., Huang, M., and Lin, J. Application of poly(acrylic acid-g-gelatin)/polypyrrole gel electrolyte in flexible quasi-solid-state dye-sensitized solar cell. *Electrochimica Acta*, 55(8):2777-2781, 2010.

[20] Lin, L. Y., Tsai, C. H., Wong, K. T., Huang, T. W., Hsieh, L., Liu, S. H., Lin, H. W., Wu, C. C., Chou, S. H., Chen, S. H., and Tsai, A. I. Organic dyes containing coplanar diphenyl-substituted dithienosilole core for efficient dye-sensitized solar cells. *Journal of Organic Chemistry*, 75(14):4778-4785, 2010.

[21] Huo, Z., Dai, S., Zhang, C., Kong, F., Fang, X., Guo, L., Liu, W., Hu, L., Pan, X., and Wang, K. Low molecular mass organogelator based gel electrolyte with effective charge transport property for long-term stable quasi-solid-state dye-sensitized solar cells. *Journal of Physical Chemistry B*, 112(41):12927-12933, 2008.

[22] Wu, C., Jia, L., Guo, S., Han, S., Chi, B., Pu, J., and Jian, L. Open-circuit voltage enhancement on the basis of polymer gel electrolyte for a highly stable dye-sensitized solar cell. *ACS Applied Materials and Interfaces*, 5(16):7886-7892, 2013.

[23] Barea, E. M., Ortiz, J., Payá, F.J., Fernández-Lázaro, F., Fabregat-Santiago, F., Sastre-Santos, A., and Bisquert, J. Energetic factors governing injection, regeneration and recombination in dye solar cells with phthalocyanine sensitizers. *Energy and Environmental Science*, 3(12):1985-1994, 2010.

[24] Bisquert, J. Chemical capacitance of nanostructured semiconductors: Its origin and

significance for nanocomposite solar cells. *Physical Chemistry Chemical Physics*, 5(24):5360-5364, 2003.

[25] Bisquert, J., Grätzel, M., Wang, Q., and Fabregat-Santiago, F. Three-channel transmission line impedance model for mesoscopic oxide electrodes functionalized with a conductive coating. *Journal of Physical Chemistry B*, 110(23):11284-11290, 2006.

[26] Bisquert, J. Theory of the impedance of electron diffusion and recombination in a thin layer. *Journal of Physical Chemistry B*, 106(2):325-333, 2002.

[27] Adachi, M., Sakamoto, M., Jiu, J., Ogata, Y., and Isoda, S. Determination of parameters of electron transport in dye-sensitized solar cells using electrochemical impedance spectroscopy. *Journal of Physical Chemistry B*, 110(28):13872-13880, 2006.

[28] Yu, J., Fan, J., and Lv, K. Anatase TiO_2 nanosheets with exposed (001) facets: Improved photoelectric conversion efficiency in dye-sensitized solar cells. *Nanoscale*, 2(10):2144-2149, 2010.

[29] Liu, Y., Hagfeldt, A., Xiao, X. R., and Lindquist, S. E. Investigation of influence of redox species on the interfacial energetics of a dye - sensitized nanoporous TiO_2 solar cell. *Solar Energy Materials and Solar Cells*, 55(3):267-281, 1998.

[30] Lyon, L. A. and Hupp, J. T. Energetics of semiconductor electrode/solution interfaces: EQCM evidence for charge-compensating cation adsorption and intercalation during accumulation layer formation in the titanium dioxide/acetonitrile system. *Journal of Physical Chemistry*, 99(43):15718-15720, 1995.

[31] Redmond, G. and Fitzmaurice, D. Spectroscopic determination of flatband potentials for polycrystalline titania electrodes in nonaqueous solvents. *The Journal of Physical Chemistry*, 97(7):1426-1430, 1993.